EPJ Web of Conferences **265**, 00040 (2022) https://doi.org/10.1051/epjconf/202226500040
Multi-line Diagnostics of the Interstellar Medium

AB Aur: A Rosetta stone for planet formation theories

Pablo Rivière-Marichalar[1,*]

[1]Observatorio Astronómico Nacional (OAN,IGN), Calle Alfonso XII, 3. 28014 Madrid, Spain

Abstract. AB Aur is a Herbig Ae star that hosts a well-known protoplanetary disk that depicts a plethora of features that can be attributed to the presence of a forming planet, such as a large inner cavity, a dust trap, and spiral arms. We present NOEMA observations of molecular species towards this transition disk around AB Aur, including CO, ^{13}CO, C^{18}O, HCN, HCO$^+$, SO, H_2CO, and H_2S. These observations reveal complex chemistry with strong chemical differentiation and the presence of a cavity-crossing filament.

1 Introduction

Planet formation takes place in circumstellar disks made of gas and dust surrounding young stellar objects. Therefore, characterizing the physical conditions and the chemical composition of protoplanetary disks is key for understanding planet formation. AB Aur is a widely studied Herbig A0 star that hosts a transitional disk. At a distance of ∼160 pc [1], the system is well suited to study the distribution of gas and dust in circumstellar environments. The system depicts a plethora of features that can be attributed to planet formation, such as a large inner cavity [2–5], spiral arms [4, 6–8], and a dust trap [2, 5]. Low-resolution spectral observations of AB Aur are available from ∼1 μm up to ∼ 400 μm. The detection of several O I, C II, C, OH, and rovibrational lines of CO and H_2 demonstrates the existence of warm gas. The origin of these emission lines is, however, uncertain due to the moderate angular resolution of the observations. Our team is performing a large observational effort to study the dust and gas content in this interesting object [5, 8, 10].

2 Accretion within the dust cavity?

We observed AB Aur with NOEMA in 2017 [10] to map the emission from HCO$^+$ 3-2 and HCN 3-2. Velocity integrated intensity maps are shown in Fig. 1. There are prominent differences between the maps of the two species. While HCN is only detected in an annular ring spatially coincident with the dust ring, HCO$^+$ is detected in the outer ring and also features intense emission toward the central position. Furthermore, a bright HCO$^+$ emission bridge connects the outer disk with the inner structure.

We show in the top-central panel of Fig. 1 the first-moment map of HCO$^+$ J=3-2. The outer parts of the disk are close to Keplerian rotation, but twisted isophotes are observed towards the central regions (r<0.6”). It has been proposed that twisted isophotes can be reproduced using either two misaligned Keplerian disks [7] or an outflow [12]. A simple

*e-mail: p.riviere@oan.es

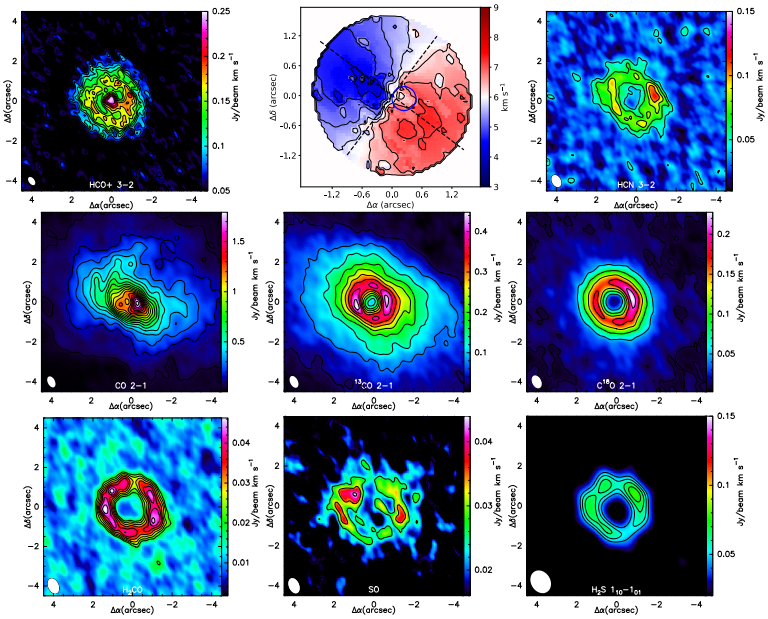

Figure 1. Top left: HCO^+ integrated intensity map. Top center: HCO^+ first moment map. The dashed lines indicate the direction of the major and minor axes. The blue circle contains a region with large anomalies with respect to a Keplerian rotation velocity field. Top right: HCN integrated intensity map. Middle and bottom panels: from left to right and top to bottom the panels show the velocity integrated intensity maps of ^{12}CO 2-1, ^{13}CO 2-1, C^{18}O 2-1, H_2CO 3_{03}-2_{02}, SO 5_6-4_5, and H_2S 1_{10}-1_{01}. Th synthetized beam is shown in the bottom left corner of each map.

model consisting of two misaligned disks provides a good fit across the disk except in the position of the bridge region, where prominent residuals are observed (see the blue circle in Fig. 1, top central panel). Visual inspection of spectra at this position demonstrates the presence of material moving at forbidden velocities, most likely infalling material moving at free-fall velocities. By including a free-fall velocity component in our model we get a much better fit to the first-moment map. At the position of the bridge, the free-fall model has a velocity of 5.5 km s^{-1}, compared to the velocity of 5.3 km s^{-1} of the blue-shifted component observed towards the bridge. Assuming that this component is due to accretion, we derived a mass accretion rate 3×10^{-8} to 3×10^{-7} $M_\odot$ yr^{-1} comparable to previous measurements [13].

3 Radial segregation of chemical species

In a later paper [8] we presented observations of ^{12}CO, ^{13}CO, C^{18}O, HCN, HCO^+, SO, and H_2CO with very different radial and azimuthal distributions. The species showed strong radial segregation, with differences as large as 100 au in the positions of their peaks. The only species that peaked toward the center was HCO^+. All the species showed emissions that were more extended than that of the dust, and the most extended species were ^{12}CO and ^{13}CO, with 5σ emission detected at distances larger than 4" due to pollution by envelope emission. It would be reasonable to postulate that this radially layered structure is related to the snow lines of the different species, which are determined by their binding energies. If thermal desorption is the main desorption mechanism in the mid-plane, the radius of the snow line

would be expected to anti-correlate with the binding energy. However, this was not true for the observed species, suggesting that thermal desorption is not the main driver of the chemical evolution of the disk. Our data reveal that different species are probing different regions of the disk and the envelope. Species such as ^{12}CO and ^{13}CO trace the disk surface and the remnant envelope. Other species, such as C^{18}O and HCN, are tracing the dusty disk, with a radial profile that almost overlaps with that of the continuum. H_2CO and SO trace the outer regions of the disk. The differences observed in the radial distribution of the different species surveyed were also present in their azimuthal profiles. C^{18}O peaks close to the position of the dust trap, while SO peaks at ∼180° from the position of the dust trap, and other species such as HCN, H_2CO, and HCO^+ are mostly flat along the ring. We used the H_2CO lines observed to derive a mean gas temperature of 39 K, in good agreement with the temperature of 37 K that we obtained using SO lines. This mean temperature of 39 K is larger than the typical value for disks around T Tauri stars. We derived a gas-to-dust map of the disk by combining observations of ^{13}CO, C^{18}O, and continuum emission at 1 mm. The mean gas-to-dust ratio of the disk was 40, well below the canonical value of 100 assumed for the ISM.

We computed a set of six 1+1D Nautilus simulations [14] to compare with the radial profiles of the observed species [8]. Nautilus is a time-dependant, three-phase astrochemical model in which gas, grain surface, and grain mantle phases are considered. We tested two values for three parameters that were relevant to the chemistry of the system: the gas-to-dust ratio (40 and 100), the C/O abundance ratio (0.7 and 1.0), and the sulfur abundance (1.5×10^{-5}, which is the cosmic abundance [17], and a depleted value of 8×10^{-8}). The high abundance of observed H_2CO favored models with a gas-to-dust ratio of 40, in agreement with the value derived from our observations. HCN is very sensitive to the C/O ratio, and its radial profile was better adjusted assuming C/O=1. The SO radial profile, however, was better reproduced by a model with strong sulfur depletion ($[S/H] = 8 \times 10^{-8}$) and C/O=0.7. This model ($[S/H] = 8 \times 10^{-8}$, C/O=0.7) did indeed reproduce all the observed column densities exception made of HCN.

4 Resolved observations of H_2S

We observed the H_2S 1_{10}-1_{01} transition with NOEMA (see the velocity integrated intensity map in Fig. 1 bottom right panel) with an angular resolution of 1.19" × 0.97" [15]. This is the second time that resolved observations of H_2S towards a protoplanetary disk were performed after the observations toward GG Tau [16]. We detected emission in a ring extending from 0.67" (∼109 au) to 1.69" (∼ 275 au) with strong azimuthal asymmetries. The position of the peak in azimuth was coincident with that of the continuum at 1 mm and C^{18}O. Both the radial and azimuthal distributions of H_2S are very similar to that of H_2CO. Our recent study of H_2S emission toward young stars in Taurus identified a tentative correlation between H_2S 1_{10}-1_{01} and H_2CO 2_{11}-1_{10} velocity integrated line intensities. Our maps point to very similar spatial origins for both emission lines, providing further observational support for such correlation. The two species, H_2S and H_2CO, have formation routes on the surface of grains, a fact that could explain the correlation. Assuming LTE we derived a mean H_2S abundance with respect to H nuclei of $(1.9\pm0.4)\times10^{13}$ cm^{-2}

To study the sulfur budget in the disk we produced a Nautilus model. Given the moderate angular resolution of our data, we focused on the vertical profile at a radius r=200 au, representative of the H_2S emission ring. The model is based on the one that we used previously (see Sect. 3) to study the chemical segregation of species in the disk [8]. We assumed a gas-to-dust ratio of 40, no sulfur depletion ($[S/H] = 1.5 \times 10^{-5}$), and C/O=0.7. The details of the model can be found in the original papers [8, 15]. Our model results in an H_2S column density of 3.5×10^{13} cm^{-2}, in good agreement, given the uncertainties, with the value

derived assuming LTE. Furthermore, assuming LTE we derived an SO mean abundance of 3.2×10^{-9} cm^{-2}, again in good agreement with an abundance of 9.8×10^{-9} predicted by our Nautilus model. Our model showed that 99.99% of H_2S is locked in the surface of dust grains. Furthermore, 90.5% of the total sulfur content is locked in the surface of grains, and 98% of the sulfur content is contained in only six species: H_2S, SO_2, H_2S_3, and CS_2 in the surface of grains and gaseous S and S^+. Gaseous species (S and S^+) become relevant only at around 15 au over the mid-plane, where the visual extinction is only 1.5 mag. Regarding the overall composition of the grain surfaces, H_2S is the third most abundant species in the model after H_2O and CO, which highlights the importance of these species for the chemistry of protoplanetary disks.

5 Summary

The AB Aur protoplanetary disk presents a series of features that makes it a good candidate to look for young and embedded forming planets, including a cavity in the inner disk, a dust trap, and spiral arms. We are driving a large observational effort using the NOEMA observatory to characterize the gaseous content of this system. Observations of HCO^+ revealed the presence of a filamentary structure that is crossing the cavity, connecting the inner and outer disk. The material in this bridge appears to be moving at free-fall velocities and it is likely tracing material being accreted onto the central source. Our NOEMA observations point to strong radial segregation of chemical species in the disk. The positions of the peaks in the radial profiles of the surveyed species suggest that thermal desorption is not driving the chemical evolution of the disk. We derived a mean gas-to-dust ratio of 40, significantly smaller than the canonical value of 100 assumed for the ISM, in agreement with recent studies of the gas content of protoplanetary disks. We further used observations of H_2CO and SO to estimate a mean temperature of 39 K for the gas in the disk. Finally, we used observations of SO and H_2S to study the sulfur budget in the disk. According to our NAUTILUS model, H_2S is the main sulfur carrier on the surface of grains. Future observations with NOEMA will help us to grow our database to study the protoplanetary disk around AB Aur.

References

[1] Gaia collaboration, Vizier Online Data Catalog, I345 (2018)
[2] Piétu, V., Guilloteau, S., Durtey, A., A&A **443**, 945-954 (2005)
[3] Tang, Y. -W., Guilloteau, S., Piétu, V., et al., A&A **547**, A84 (2012)
[4] Tang, Y. -W., Guilloteau, S., Durtey, A., et al., ApJ **84**, 32 (2017)
[5] Fuente, A., Barutearu, C., Neri, R., et al., A&A **846**, L3 (2017)
[6] Fukagawa, M., Hayashi, M., Tamura, M., et al., ApJL **605**, L53-L56 (2004)
[7] Hashimoto, J., Tamura, M., Muto, T., et al., ApJ **729**, L17 (2011)
[8] Rivière-Marichalar, P., Fuente, A., Le Gal, R., et al., A&A **642**, A32 (2020)
[9] Fuente, A., Cernicharo, J., Agúndez, M., et al., A&A **524**, A19 (2010)
[10] Rivière-Marichalar, P., Fuente., A., Baruteau, C., et al., ApJL **879**, L14 (2019)
[11] Rodríguez, L. F., Zapata, L., A., Dzib, S. A., et al., ApJ **793**, L21 2014
[12] Rosenfeld, K., A., Chiang, E., Andrew, S. M., ApJ **782**, 62 (2014)
[13] Salyk, C., Herczeg, G. J., Brown, J. M., et al., ApJ **769**, 21 (2013)
[14] Wakelam, V., Ruaud, M., Hersant, F., et al., A&A **594**, A35 (2016)
[15] Rivière-Marichalar, P., Fuente, A., Esplugues, G., A&A, submitted.
[16] Phuong, N. T., Chapillon, E., Majumdar, L., et al., A&A **616**, L5 (2018)
[17] Daflon, S., Cunha, K., de la Reza, R., et al., AJ **138**, 1577-1583 (2009)